Materials Research. 2021; 24(2): e20200401
DOI: https://doi.org/10.1590/1980-5373-MR-2020-0401

A Characterization of Hot Flow Behaviors of Invar36 Alloy by an Artificial Neural Network with Back-Propagation Algorithm

Zhen-yu Zou[a]*, Tao Li[a], Xiao-bo Zhang[a], Wei-tao Zheng[a], Yi Zhang[a], Yong-bing Zhang[a]

[a]AVIC Chengdu Aircraft Industrial (Group) Co., Ltd, Chengdu, China

Received: September 3, 2020; Revised: December 27, 2020; Accepted: January 25, 2021

In order to investigate the hot deformation behaviors of Invar36 alloy, isothermal compressive tests were conducted on a Gleeble 1500 thermo-mechanical simulator at the temperatures of 873, 948, 1023, 1098 and 1173 K and the strain rates of 0.01, 0.1, 1 and 10 s^{-1}. The effects of strain, temperature and strain rate on flow stress were analyzed, and a dynamic recrystallization type softening characteristic with unimodal flow behavior is determined. An artificial neural network based on back-propagation algorithm was proposed to handle the complex deformation behavior characteristics. The ANN model was evaluated in terms of correlation coefficient and average absolute relative error. A comparative study was performed on ANN model and constitutive equation by regression method for Invar36 alloy. Finally, the ANN model was applied to the finite element simulation, and an experimental study on trial hot forming of a V-shaped part was conducted to demonstrate the precision of the finite element simulation based on predicted flow stress data by ANN model. The results have sufficiently showed that the well-trained ANN model with BP algorithm is able to deal with the complex flow behaviors of Invar36 alloy and has great application potentiality in hot deformation.

Keywords: *Invar36 Alloy, artificial neural network, constitutive equation, finite element simulation.*

1. Introduction

As a special functional material, Invar36 alloy is especially attractive for electronics industry, LNG storage tanks, long-distance power transmission lines, the forming mold of composite material and other fields on account of its extremely low coefficient of thermal expansion (CTE) below Curie temperature[1-3]. It is well known that the deformation behaviors of metals in hot forming process, significantly affected by the deformation parameters including strain, strain rate and temperature, have an important influence on the dimensional accuracy and mechanical properties of final products. In the process of plastic deformation under various conditions, a variety of interrelated metallurgical phenomena including work hardening (WH), dynamic recrystallization (DRX) and dynamic recovery (DRV) coexist with one being predominant. WH increases the flow stress and reduces the plasticity, while softening phenomena like DRX and DRV decreases the flow stress and thereby increases the ductility. The metallurgical phenomena and their interactions in the hot deformation condition cause complex deformation behaviors. Therefore, the constitutive relationships between flow stress and processing parameters, contribute significantly to the deep understanding of flow behaviors and even further optimization of hot deformation process[4].

At present, the analytical constitutive models and phenomenological constitutive models are the most popular in hot flow behaviors modeling[5]. Closely connected with physical theories, the analytical model is obtained based on a large amount of experimental data through a very clear and deep understanding of flow behaviors and deformation mechanisms of metallic materials, making it difficult to analyze the constitutive relationships under limited experimental conditions. However, the phenomenological model, which is less rigorously related to physical theories in comparison with the analytical model, is widely adopted for effective flow behaviors modeling. Typical phenomenological models are using regression method to develop the constitutive equations, including the Arrhenius-type constitutive equations based on exponential law, power exponential law and hyperbolic sine law[6], in which only a reasonable number of constants need to be calculated through regression analysis with a limited amount of experimental data. However, these phenomenological models are not quite satisfied due to the low accuracy in predicting the highly nonlinear constitutive relationships of the metallic materials in a very large parameter range.

Compared with regression method, the artificial neural network (ANN), as a relatively new Artificial intelligence algorithm, is able to solve the complex problems well by means of simulating the behavior of biological neural systems in computers[7]. This approach makes it possible to manage the constitutive relationships of the flow stress, strain, strain rate and temperature with a collection of representative examples from the expected mapping functions for training instead of a well-defined mathematical model[8-10]. As a result, the flow stress can be predicted through the constitutive model obtained by ANN method. For the past few decades, the description of constitutive relationships by ANN method has attracted many researchers. Peng et al. compared the

*e-mail: zzy0518@msn.cn

constitutive relationships of as-cast Ti60 titanium alloy through Arrhenius-type and ANN model[11]. Zhu et al. successfully developed an ANN model to predict the flow stress of as-cast TC21 titanium alloy[6]. Quan et al. developed an ANN constitutive model of as-forged Ti-10V-2Fe-3Al alloy in a wide temperature range involving phase transformation[12] and Lin et al. established the optimized hot forming processing parameters for 42CrMo steel on basis of ANN model[13]. The results of stress prediction in these researches agree well with the experimental data, indicating that ANN is an effective tool available to model the highly nonlinear constitutive relationships of metallic materials.

Aiming at developing an ANN constitutive model for Invar36 alloy using back-propagation algorithm, twenty compression tests were performed at different temperatures and strain rates in present work. The stress-strain data collected in the compression tests were used to develop the artificial neural network model. The evaluation of ANN model has been conducted by several statistical parameters. A three-dimensional plot for the semi-continuous visualized description of the constitutive model was developed based on several groups of flow stresses at different strain rates and different temperature conditions predicted by the well trained ANN model. Subsequently, a comparative analysis to evaluate the ANN model and the constitutive equation by regression method has been conducted based on standard statistical parameters. The results reveal that the ANN model has better accuracy and it is more excellent to model the flow behaviors of Invar36 alloy.

As the well-trained ANN model could provide a wide range of flow stress data, it can be applied in numerical simulation with high accuracy. Quan et al. developed an ANN model for 42CrMo high strength steel and improved the accuracy of finite element method (FEM) simulation by importing a wide range of stress-strain data predicted by the ANN model[14]. In current work, the ANN model for Invar36 alloy was successfully applied to numerical simulation by using FEM on DEFORM-3D software, and the dependability of finite element simulation based on stress-strain data predicted by ANN model has been demonstrated through a hot forming experiment of a V-shaped part.

2. Materials and Experimental Procedure

The chemical compositions (wt.%) of Invar36 alloy used in the current investigation are as follows: Ni-36, C-0.01, Si-0.2, Mn-0.3, S-0.002, P-0.007, Cr-0.15, Co-0.4, Fe (balance). The homogenized sheet was scalped to 20 cylindrical specimens with a diameter of 8 mm and a height of 12 mm. All the specimens were homogenized under temperature 1033 K for one hour. Before compression tests, two thermocouple wires were welded on two spots with a distance of 1mm at the mid-span of each billet where a temperature differential is experienced by the two different conductors. Subsequently, the specimens were placed in a servohydraulic Gleeble 1500 thermomechanical simulator, and then resistance heated at a heating rate of 5 K/s and held at a fixed temperature for 180 s by thermo-coupled feedback-controlled AC current, which decreased the material anisotropy in flow behaviors effectively. Next, all the 20 specimens were compressed to a fixed true strain of 0.9 (height reduction of 60%) at five different temperatures of 873, 948, 1023, 1098 and 1173 K and four different strain rates of 0.01, 0.1, 1 and 10 s^{-1}.

During these compressions, the variations of nominal stress and nominal strain were monitored continuously by a personal computer equipped with an automatic data acquisition system during the compression process. The true stress and true strain were derived from the measurement of the nominal stress-strain relationships according to the following formula: $\sigma_T = \sigma_N(1+\varepsilon_N)$, $\varepsilon_T = \ln(1+\varepsilon_N)$, where σ_T is true stress, σ_N is nominal stress, ε_T is true strain and ε_N is nominal strain.

3. Results and Discussion

3.1. Flow behavior characteristics of Invar36 alloy

The true compressive stress-strain curves of Invar36 alloy recorded automatically in the isothermal compression process are shown as Figure 1. The shapes of the stress-strain curves are sensitively dependent on temperature, strain and strain rate. Comparing these curves with one another, it is found that the stress level decreases with temperature increasing or strain rate decreasing. It is induced by the fact that lower strain rate and higher temperature provide more time for energy accumulation and higher mobilities at boundaries that result in nucleation and growth of dynamically recrystallized grains and dislocation annihilation[15,16].

It can be summarized from all the true stress-strain curves that there are two kinds of variation tendencies in the stress evolution with strain. At compression conditions of 1098 K–1173 K and 0.01 s^{-1}-0.1 s^{-1}, the flow stress curves are characterized by a single peak followed by a continuous descent towards a steady state, which exhibits the occurrence of DRX during hot deformation. At the compression conditions of 873 K–1023 K and 0.01 s^{-1}-0.1 s^{-1}, 873 K-1173 K and 0.01 s^{-1}-10 s^{-1}, the flow stress curves are characterized by a steady state without any peak, which is commonly accepted the process of DRV. In summary, as for Invar36 alloy, the response of stress to the three deformation parameters including strain, strain rate and temperature shows highly nonlinear behaviors.

3.2. Development of ANN model for Invar36 alloy

3.2.1. ANN model

The back-propagation (BP) algorithm, one of the most efficient learning algorithms for the multilayer feed-forward artificial neuron networks in materials modeling, was employed in this research to get a good understanding of the constitutive relationships between the inputs and outputs since it is a typical means of adjusting the weights and biases by gradient descent to minimize the target error[17] and it has a great representational power for dealing with complex and strongly coupled relationships[18].

The structure of ANN applied in present work was schematically illustrated in Figure 2. The input variables in this investigation include deformation temperature (T), strain (ε) and strain rate ($\dot{\varepsilon}$), while the output variable is flow stress (σ), as shown in Figure 2. In addition, two hidden

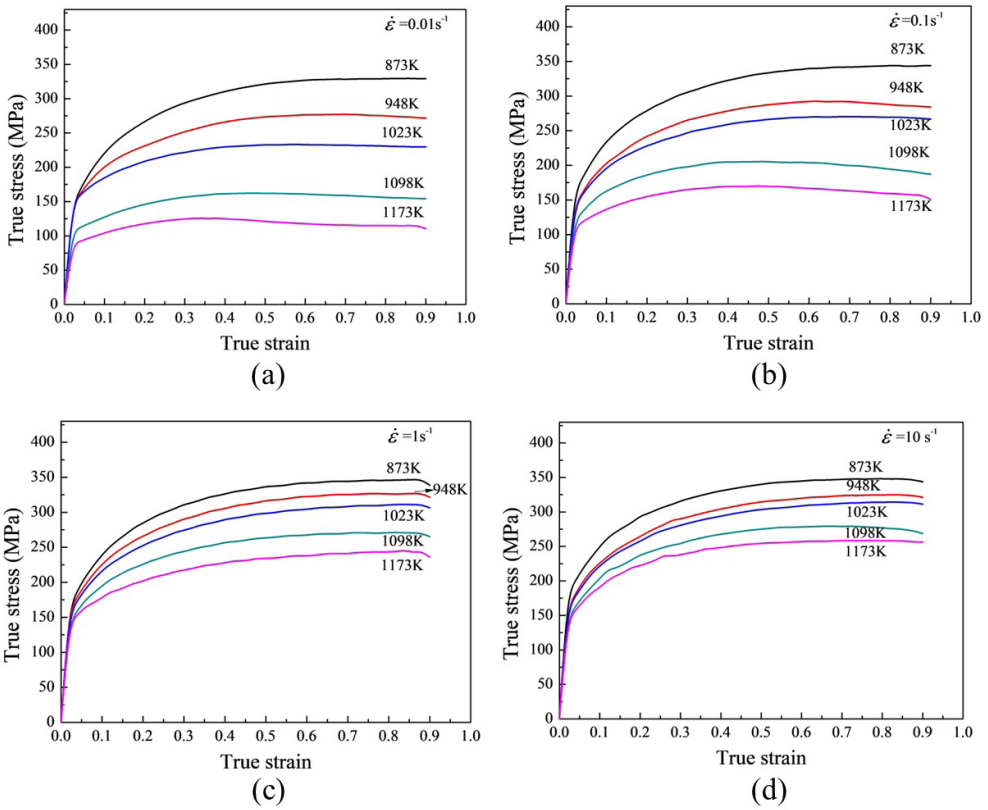

Figure 1. The true stress-strain curves of Invar36 alloy under the different temperature with strain rates of (a) 0.01 s^{-1}, (b) 0.1 s^{-1}, (c) 1 s^{-1} and (d) 10 s^{-1}.

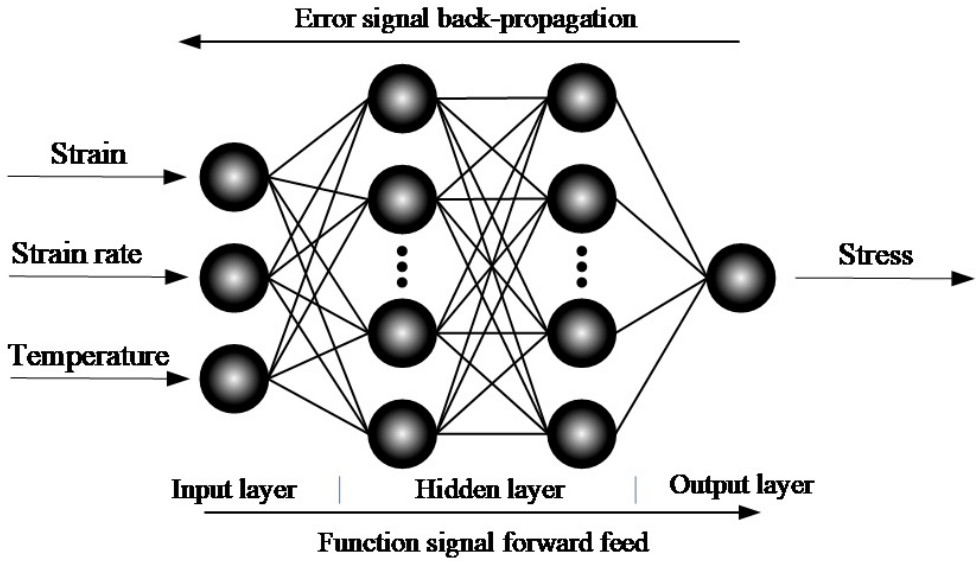

Figure 2. Schematic illustration of the neural network architecture.

layers were adopted to ensure the accuracy of ANN model. About 900 regular datasets have been extracted from the 20 stress-strain curves, in which the datasets at strain of 0.1, 0.2, 0.3, 0.4, 0.5, 0.6, 0.7, 0.8 and 0.9 were chosen as the testing sets, while the datasets remained were used to train the model. The experimental data including temperature, strain, strain rate and stress were measured in different units, which may result in the decrease of the convergence speed and accuracy of the model. As a result, the input and output variables should be normalized into dimensionless units before training to reduce the effects caused by different units. It can be found from the stress-strain data that the input

strain data vary from 0.02 to 0.9, strain rate data vary from 0.01 s^{-1} to 10 s^{-1}, and temperature data vary from 873 K to 1173 K, the output flow stress data vary from 87.44 MPa to 348.14 MPa. The data of temperature, strain and the flow stress were normalized within the range from 0.05 to 0.3 using the relation given by Equation 1. Meanwhile, the strain rate data, after taking logarithm of the values, were normalized by the relation of Equation 2, since the range of the data is much too wide.

$$y_n = 0.05 + 0.25 \times \frac{y - 0.95y_{\min}}{1.05y_{\max} - 0.95y_{\min}} \quad (1)$$

$$y_n = 0.05 + 0.25 \times \frac{(3+y) - 0.95(3+y_{\min})}{1.05(3+y_{\max}) - 0.95(3+y_{\min})} \quad (2)$$

where y_n is the normalized value of y, y is the experimental data, $y_{\max}$ and $y_{\min}$ are the maximum and minimum value of y respectively.

The structure parameters of ANN, involving hidden layer number, transfer function, training function and neuron number for each hidden layer, is of great significance for an excellent model. Firstly, two hidden layers were adopted in current investigation to ensure high accuracy. Subsequently, an associated transfer function, which can represent how the weighted sum of its inputs is transferred to the results into outputs, was set for each layer. The selected transfer function is 'tan sigmoid' for each hidden layer, and 'pure linear' for output layer. In addition, the training function is 'trainbr'. Finally, the neuron number for each hidden layer was set by means of trail-and-error method according to experience and the training sample size. If the neuron number of each hidden layer in ANN model is too small, the model may be insufficient to learn the process correctly in training process. On the contrary, too many neurons may slow down the convergence rates or over fit the data. The ANN model in current research was trained firstly with 3 neurons in each hidden layer, and then the neuron number was adjusted continually to 18 for the purpose of approaching the expected accuracy.

3.2.2. Evaluation of the performance of the ANN model

The value of mean square error *(MSE),* expressed by Equation 3[18], is introduced to evaluate the ability of the ANN training work and determine the neuron number for each hidden layer.

$$MSE = \frac{1}{N}\sum_{i=1}^{N}(E_i - P_i)^2 \quad (3)$$

where E is the sample of experimental value, P is the sample of predicted value by ANN model, N is the number of stress-strain samples.

The *MSE*-value of each actual training work was calculated as the training work of ANN models with different neuron number was accomplished. As a result, the *MSE* values of the models are in the range of 0.0000262 to 0.00000014. In order to obviously exhibit the small differences and variation trend with different neuron numbers, the *MSE* values were measured in logarithm, as shown in Figure 3. It is obviously been found in Figure 3 that the *MSE* decreases to a minimum value when the neuron number in each hidden layer is 13, showing that the ANN model with 13 neurons in each hidden layer shows excellent performance.

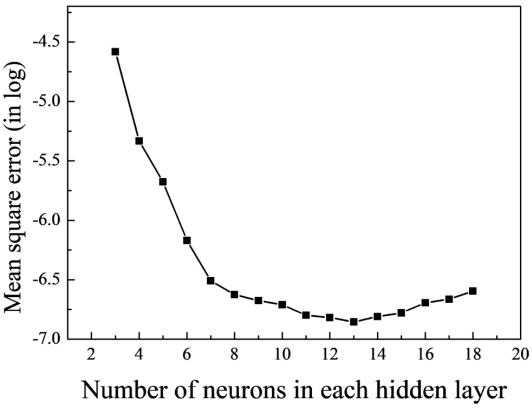

Figure 3. Performance of the network at different hidden neurons level.

As the ANN model with 13 neurons in each hidden layer had been well trained, the performance was measured in terms of the correlation coefficient (R) and the average absolute relative error ($AARE$)[18-20], as expressed by Equation 4 and Equation 5, respectively. The correlation coefficient is a widely used in measuring the strength of linear relationships between experimental and predicted values, while the average absolute relative error indicates the accuracy of the prediction. Low level of *AARE*-values and high level of *R*-values indicate that the predicted values of flow stress agree very well with the experimental value.

$$R = \frac{\sum_{i=1}^{N}(E_i - \overline{E})(P_i - \overline{P})}{\sqrt{\sum_{i=1}^{N}(E_i - \overline{E})^2 \sum_{i=1}^{N}(P_i - \overline{P})^2}} \quad (4)$$

$$AARE(\%) = \frac{1}{N}\sum_{i=1}^{N}\left|\frac{E_i - P_i}{E_i}\right| \times 100 \quad (5)$$

where E is the sample of experimental value, P is the sample of predicted value by ANN model, $\overline{E}$ and $\overline{P}$ are the mean value of E and P respectively, N is the number of stress-strain samples.

Figure 4a and b shows the correlation relationships of experimental and predicted values for the training procedure and testing procedure, respectively. As shown in Figure 4, the correlation coefficient (R) values for the training procedure and testing procedure were calculated to be 0.99998 and 0.99979, respectively. Meanwhile the *AARE* values for the training procedure and testing procedure were calculated to be determined percent of 0.1190 and 0.2638, respectively. The excellent *AARE* values and *R*-values indicate a good correlation between experimental and predicted flow stress values by the ANN model, indicating that the well-trained ANN model has reached the ideal accuracy and is able to predict the flow behaviors of Invar36 alloy well.

As the well-trained ANN model has reached excellent accuracy, it can be adopted to predict the flow stress in a wide range of processing parameter. Figure 5 shows the comparison between the datasets predicted by ANN model and the stress-strain curves obtained from compression tests.

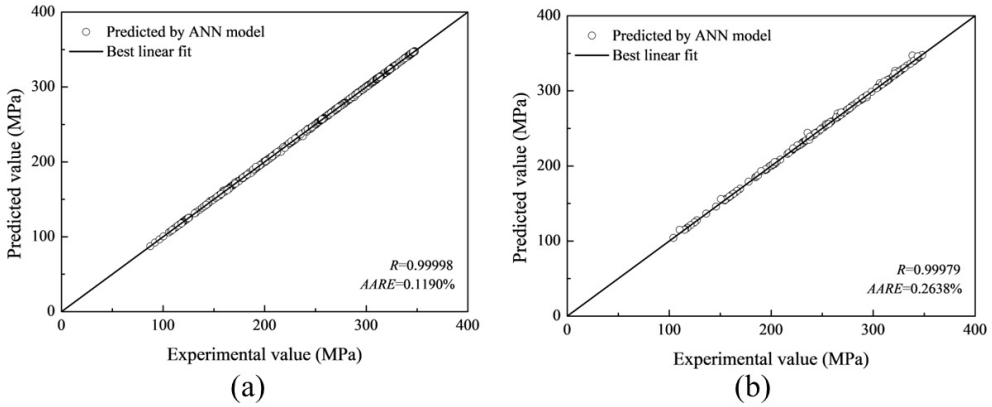

Figure 4. Correlation between experimental and predicted flow stresses for (a) the training procedure and (b) the testing procedure.

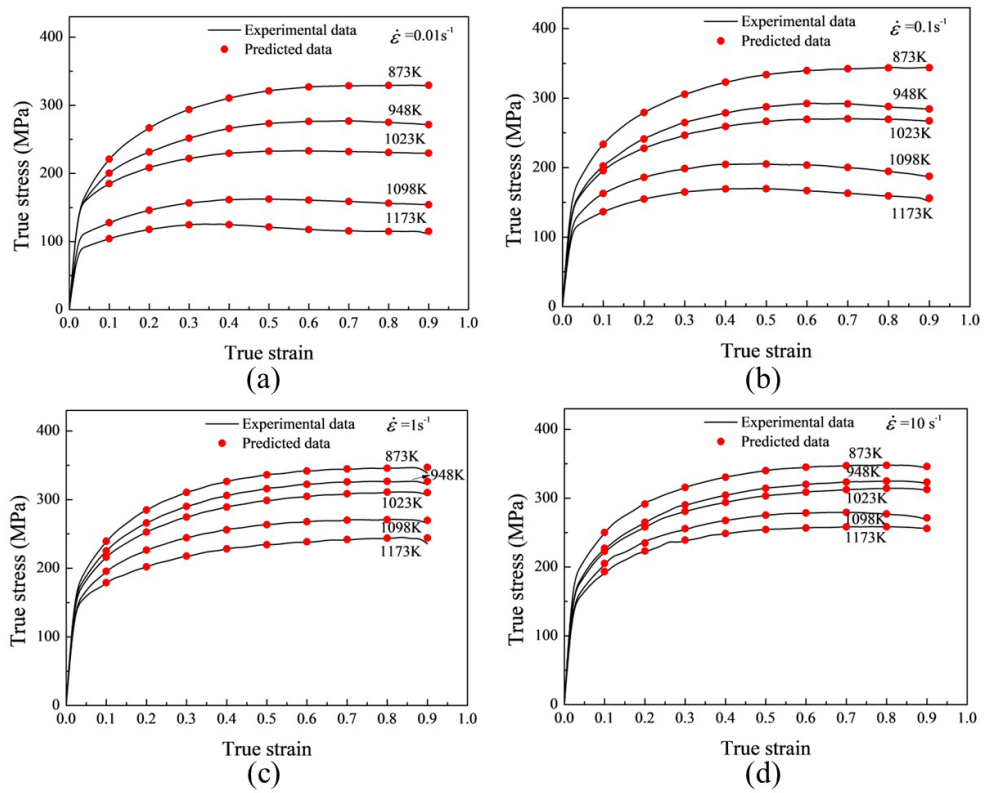

Figure 5. Comparison between the experimental and predicted flow stresses by ANN model at different temperatures and strain rates of (a) 0.01 s^{-1}, (b) 0.1 s^{-1}, (c) 1 s^{-1} and (d) 10 s^{-1}.

It is obviously been found in Figure 5 that the predicted datasets matches well with the experimental curves in a wide temperature range of 873~1173 K, a wide strain rate range of 0.01~10 s^{-1}, and a wide strain range of 0.1~0.9.

3.2.3. Generalization capability of ANN model

As stated above, the well-trained ANN model for Invar36 alloy is efficient in flow behavior modeling under limited experimental data. For the purpose of measuring the generalization capability of the well-trained ANN model for Invar36 alloy, several groups of flow stress data in and out of experimental conditions were predicted by the well-trained ANN model. Taking the datasets at temperature range of 873–1173 K with an interval of 37.5 K, logarithm strain rate range from–2 to 1 with an interval of 0.5, and strain range from 0.05 to 0.9 with an interval of 0.05 as input data, the corresponding flow stress data were outputted through the well-trained ANN model. Figure 6 shows the stress–strain curves of Invar36 alloy in and out of experimental conditions predicted by the ANN model. It can be noticed that the predicted stress curves articulate similar intrinsic characteristics with experimental strain–stress curves. In addition, a 3D plot for

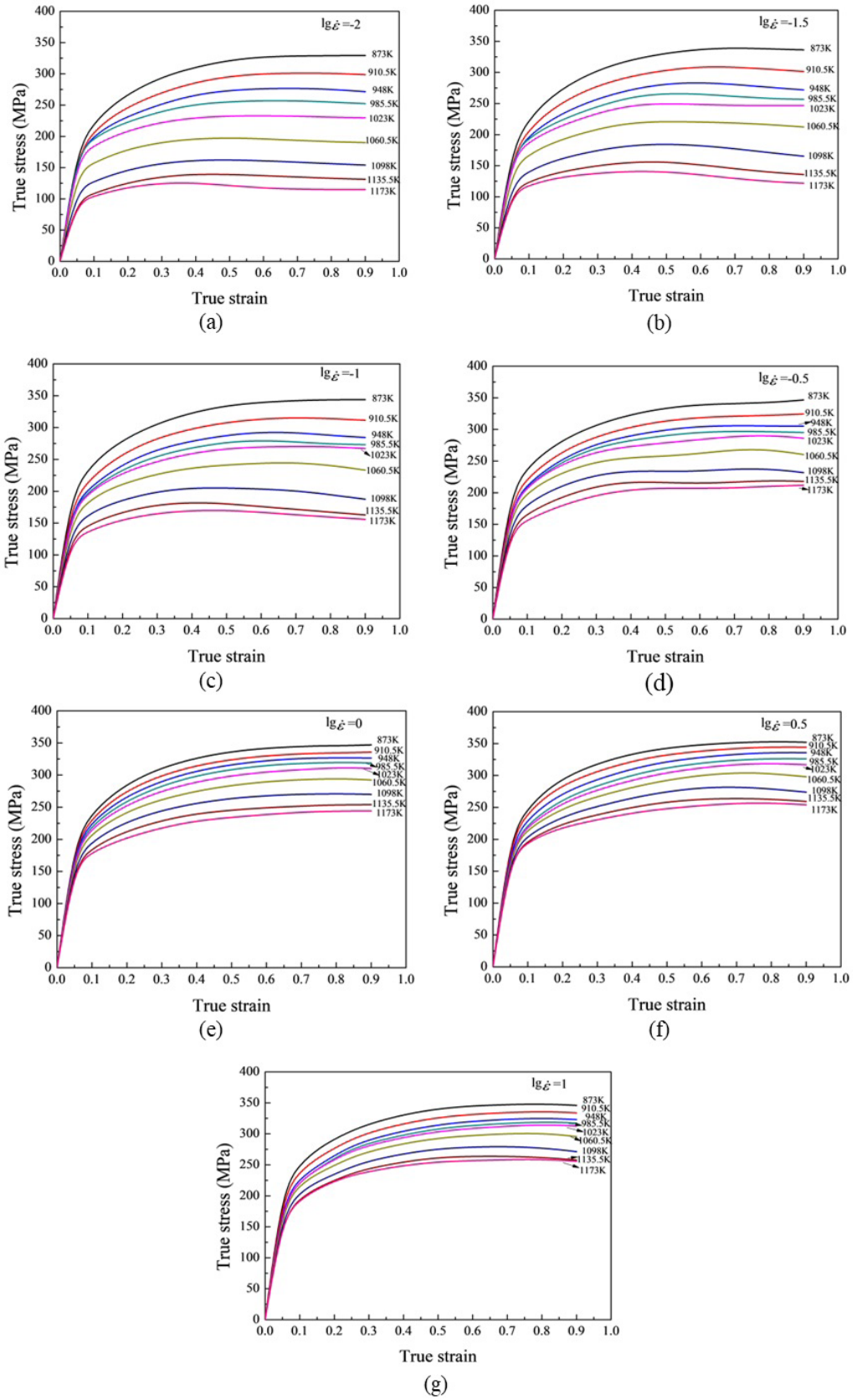

Figure 6. The true stress–strain curves of Invar36 alloy in and out of experimental conditions predicted by the well-trained ANN model with logarithm of strain rate (a) –2, (b) –1.5, (c) –1, (d) –0.5, (e) 0, (f) 0.5 and (g) 1.

the semi-continuous visualized description of the ANN model within the temperature range of 873–1173 K, logarithm strain rate ranging from –2 to 1 and strain range from 0.05 to 0.9 were developed, as shown in Figure 7. In Figure 7, the axes of X, Y and Z represent the strain rate in log, temperature and strain, respectively. Meanwhile, the level of flow stress was measured in different colors, as shown on the color bar. The 3D plot visually reflects the variation of flow stresses with the variation of temperature, strain and strain rate. The increase of temperature, as well as the decrease of strain rate, results in the decrease of stress level. The variation of flow stresses matches well with the characteristic of experimental flow curves within the temperature range of 873–1173 K, logarithm strain rate ranging from –2 to 1 and strain range from 0.05 to 0.9, indicating a good generalization capability of the ANN model for Invar36 alloy in this investigation.

3.3. Comparison of constitutive equation by regression method and ANN model for Invar36 alloy

3.3.1. Constitutive relationship by regression method for Invar36 alloy

It is widely known that the constitutive equation between the steady-state flow stress, strain rate and deformation temperature are represented by Zener-Hollomon parameter in an exponent-type equation, and the hyperbolic law in the Arrhenius type equation gives better approximations between Z parameter and stress, as expressed in Equation 6[21-24]

$$Z = \dot{\varepsilon}\exp(\frac{Q}{RT}) = AF(\sigma) \tag{6}$$

where,

$$F(\sigma) = \begin{cases} \sigma^m & \alpha\sigma < 0.8 \\ \exp(\beta\sigma) & \alpha\sigma > 1.2 \\ [\sinh(\alpha\sigma)]^n & for\ all\ \sigma \end{cases}$$

in which, $\dot{\varepsilon}$ is the strain rate (s^{-1}), R is the universal gas constant (8.314 $J{\cdot}mol^{-1}{\cdot}K^{-1}$), T is the absolute temperature (K), Q is the apparent activation energy for hot deformation ($kJ{\cdot}mol^{-1}$), σ is the flow stress (MPa) for a given stain, A, α and n are the material constants, $\alpha = \beta/m$.

The constitutive model by regression method for Invar36 alloy was obtained in the form as Equation 6 through nonlinear multivariate regression analysis. The experimental datasets involving deformation temperature, strain rate and stress at strain of 0.5 were fitted into Equation 6. The relationships between $\ln\dot{\varepsilon} - \ln\sigma$, $\ln\dot{\varepsilon} - \sigma$, $\ln\dot{\varepsilon} - ln[sinh(\alpha\sigma)]$ and $ln[sinh(\alpha\sigma)] - 10000/T$ in $\alpha+\beta$-phase temperature range are shown in Figure 8. The value of m and β was obtained through taking average slope of the lines in Figure 8a and Figure 8b respectively. Thus the α value was calculated to be 0.003404. Subsequently, the calculation of n and Q has been performed according to the following relationships:

$$Q = Rns \tag{7}$$

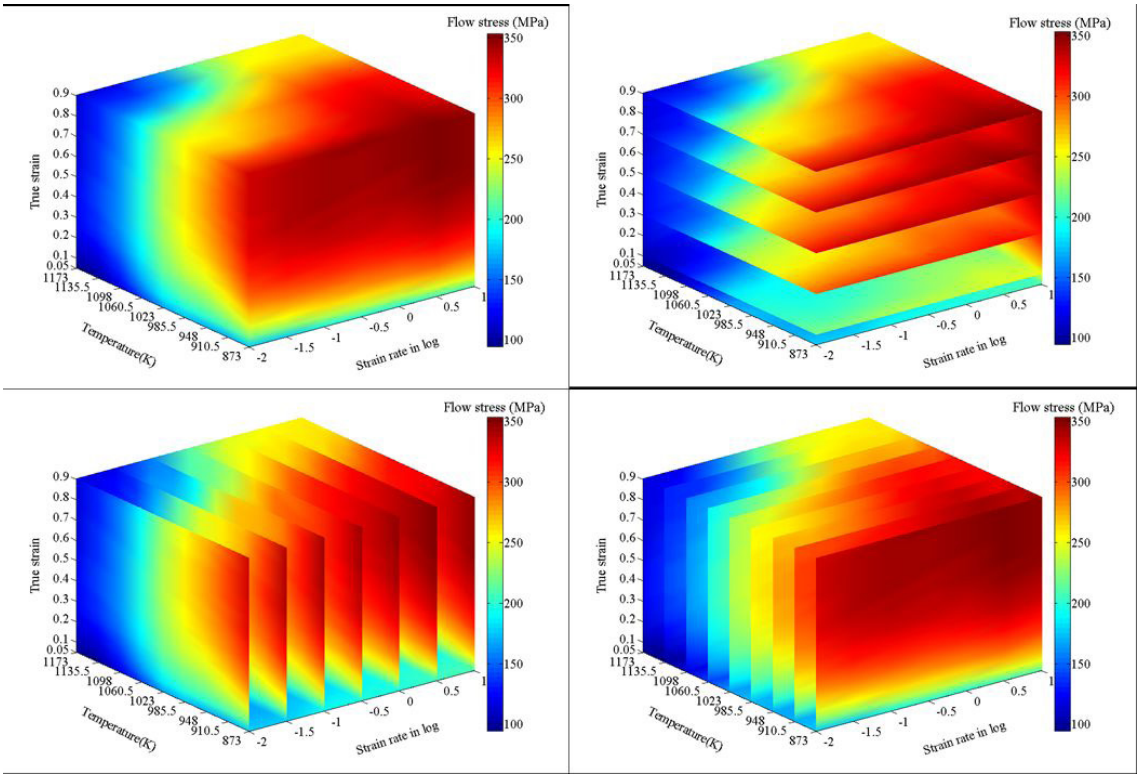

Figure 7. The 3D plot of flow stress within the temperature range of 873–1173 K, logarithm strain rate range from –2 to 1 and strain range from 0.05 to 0.9.

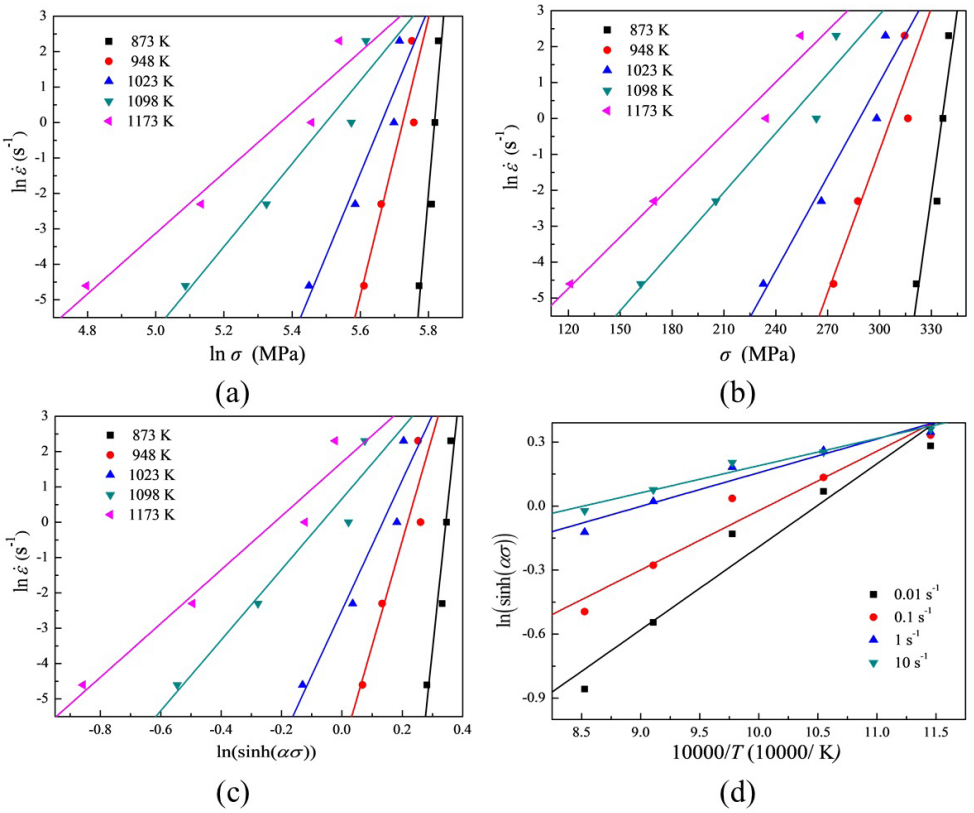

Figure 8. Relationships between (a) $\ln\dot{\varepsilon}-\ln\sigma$, (b) $\ln\dot{\varepsilon}-\sigma$, (c) $\ln\dot{\varepsilon}-ln\left(sinh\left(\alpha\sigma\right)\right)$, (d) $ln\left(sinh\left(\alpha\sigma\right)\right)-10000/T$ at strain of 0.5.

$$n=\frac{d\ln\dot{\varepsilon}}{d\ln[\sinh(\alpha\sigma)]} \tag{8}$$

$$s=\frac{d\ln[\sinh(\alpha\sigma)]}{d(1/T)} \tag{9}$$

Hence the value of n and Q was calculated to be 29.4212 and 582.479 kJ/mol respectively from the slope of the lines in Figure8c and Figure 8d. The value of A was then obtained to be 3.312×10^{29} from the intercept of the fitted line in Figure 9. Finally, the constitutive equation by regression method at strain of 0.5 can be presented as Equation 10.

$$Z=\dot{\varepsilon}\exp(\frac{582.479}{RT})=3.312\times10^{29}[\sinh(0.003404\sigma)]^{29.4212} \tag{10}$$

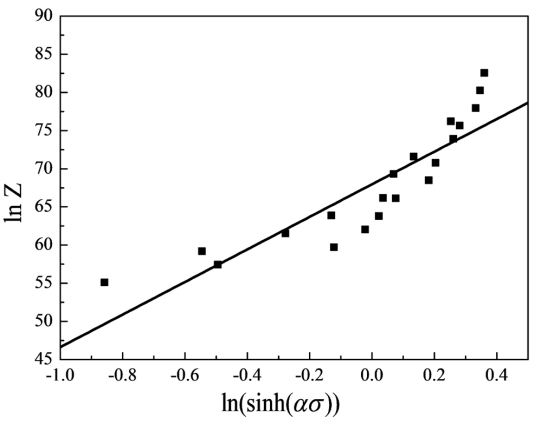

Figure 9. Variation of the Z parameter with flow stress (at strain of 0.5)

3.3.2. Comparison of the performance of the two models

Figure 10 show the correlation relationships between the experimental and predicted data at the strain of 0.5 from the regression model and the well-trained ANN model, respectively. The R-value and the *AARE*-value calculated from the ANN model is 0.99999 and 0.08599% respectively, better than the 0.90399 and 9.6735% from the regression method, indicating that the ANN model has better capacity to predict the flow behaviors of Invar36 alloy.

Additionally, as expressed by Equation 11, the relative percentage error (η) is introduced to compare different measurements of the relative difference at strain of 0.5, besides the correlation coefficient and the *AARE*.

$$\eta(\%)=\frac{P_i-E_i}{E_i}\times100\% \tag{11}$$

Where E is the sample of experimental value, P is the sample of predicted value by ANN model, N is the number of stress-strain samples.

The comparison of η-values of the ANN model and the regression model is shown in Figure 11. It can be demonstrated that the η-values obtained from ANN model vary from

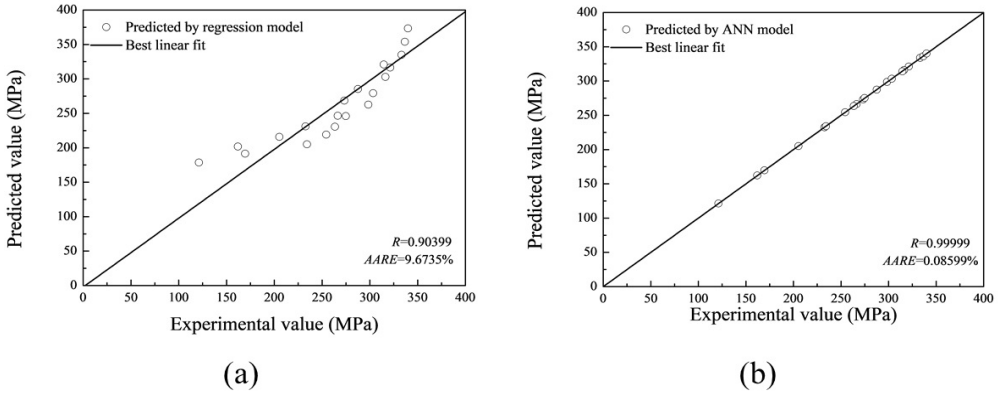

Figure 10. Correlation between experimental and predicted flow stresses at strain of 0.5 by (a) regression model and (b) ANN model.

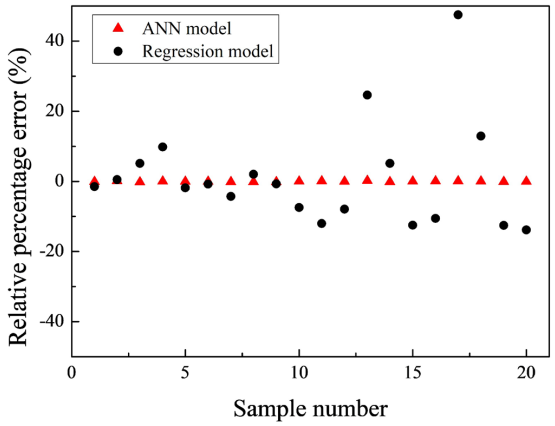

Figure 11. Comparison of relative percent error of predicted value by ANN and calculated value by regression model with experimental value at strain of 0.5.

-0.1820% to 0.1998%, whereas for the regression model, the η-values are in the range from -13.847% to 47.46%. The smaller η-value of the ANN model indicates that the predicted stress-data is closer to the experimental stress-data, i.e. the ANN model is more reliable in flow stress prediction of Invar36 alloy.

3.4. Application potentiality of ANN model in finite element simulation

3.4.1. Finite element simulation of hot forming process of a V-shaped part

As stated earlier, the flow stresses predicted by the well-trained ANN model within the temperature range of 873–1173 K, logarithm strain rate ranging from –2 to 1 and strain range from 0.05 to 0.9 agree very well with the experimental flow stress data. In current work, the flow stress data extracted from the ANN model were successfully implanted in DEFORM-3D, a commercial software of finite element analysis, since they were proved to be reliable in flow stress prediction of Invar36 alloy.

For the purpose of demonstrating the reliability of finite element simulation based on predicted flow stress data by ANN model, a hot forming process of a V-shaped part was introduced in current work. The geometry size of the V-shaped part and the 3D model of the forming die is shown in Figure 12a and 12b, respectively. The billet is an Invar36 sheet of 25.4 mm thickness with a width of 700 mm and a length of 2100 mm. The 3D finite element model of the forming process was constructed based on the thermal-mechanical multi-field coupling method, as shown in Figure 13. The top die and bottom die were set as rigid body, while the billet was set as plastic body, so as to overlook the elastic deformation and reflect the computing method of plastic yielding condition. A four-node tetrahedral finite element formulation was selected for the billet of this assembly and the movement of top die was set to hydraulic press controlled by constant speed of 5 mm/s. In addition, the physical parameters such as Initial temperature of billet, friction coefficient, heat transfer coefficient, etc. in the finite element model are listed in Table 1.

The hot forming process of the V-shaped part was simulated on software DEFORM-3D, and the results were shown in Figure 14. Figure 14a shows the distribution of the effective plastic strain. It can be clearly found from Figure 14a that the deformed work piece is inhomogeneous. On account of the friction between billet and dies, metal in top areas of the V-shape is in a free state for most of the time in the forming process and difficult to deform. Meanwhile, metal in the bottom areas of the V-shape undergoes severe deformation due to smaller deformation constraints aroused by friction. In a word, the simulation agrees well with the hot forming process of the V-shaped part. Figure 14b shows the forming load with the top die stroke of the hot forming process. The simulation load-stroke curve in the whole deformation stage shows a typical hot forming variation characteristic in which the forming load increases slowly within majority stroke of the forming process and then reaches rapidly increasing state in the last deformation stage.

3.4.2. Experimental study on trial hot forming of a V-shaped part

An Invar36 sheet of 25.4 mm thickness with a width of 700 mm and a length of 2100 mm was employed in this work and the exact chemical composition are as follows: Ni-36, C-0.01, Si-0.2, Mn-0.3, S-0.002, P-0.007, Cr-0.15, Co-0.4, Fe (balance). A set of hot forming die with cast steel

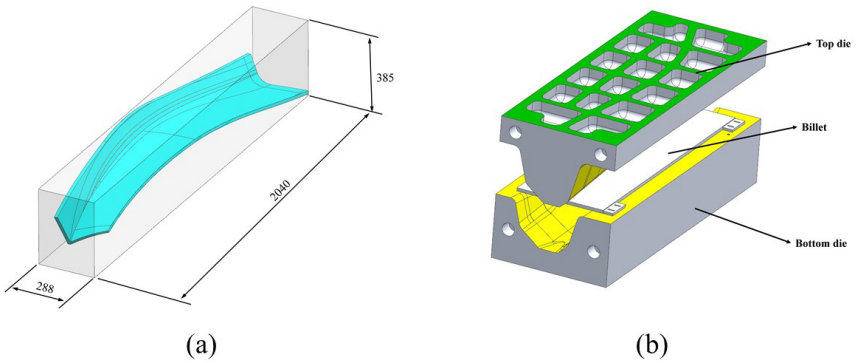

Figure 12. 3D model of (a) the V-shaped part and (b) the forming die.

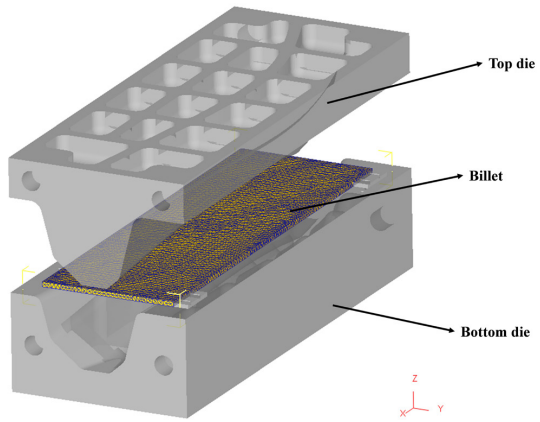

Figure 13. The finite element analytical model of the forming process of the V-shaped part.

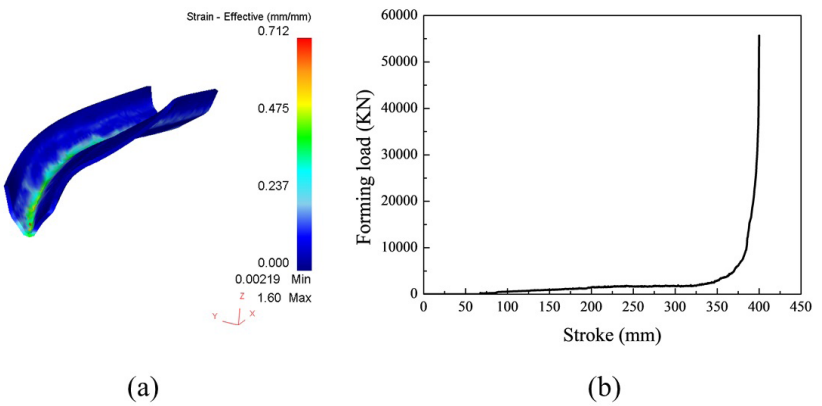

Figure 14. The simulation results of the hot forming process of the V-shaped part: (a) distribution of the effective plastic strain and (b) forming load with top die stroke.

Table 1. Physical parameters of finite element simulation.

Physical parameter		Value
Initial temperature of billet (K)		1023
Initial temperature of dies (K)		293
Environment temperature (K)		293
Friction coefficient		0.3
Heat transfer coefficient	between billet and die	5
(N/(s·mm·K)	between billet and environment	0.02

of the V-shaped part and a hydraulic press of THP10-8000 was utilized in the experiment. The speed of top die was set to 5 mm/s and the billet was heated to about 1023K, which is the same as the processing parameters in finite element model. Figure 15 and Figure 16 show the trial hot forming process of the V-shaped part and the formed V-shaped part, respectively. The forming loads were monitored continuously by a computer equipped with an automatic data acquisition system during the forming process. Figure 17 shows the comparison of logarithm load-stoke curves between experimental conditions and simulation conditions.

It is obvious that the logarithm load–stroke curve at stroke range of 100-400 mm under simulation condition matches well with the experimental logarithm load-stroke curve, and the maximum load calculated in the simulation during the final stage of the forming process is 55681.88 KN, which is much closed to the 60681.63 KN in the experiment. The finite element simulation based on predicted flow stress data by ANN model shows good performance in the case of hot forming process, which have illustrated that the well-trained ANN model is available to numerical simulation for the hot deformation behaviors with high accuracy.

(a) (b)

Figure 15. The trial hot forming process of the V-shaped part: (a) pressing process and (b) after unloading.

Figure 16. The formed V-shaped part.

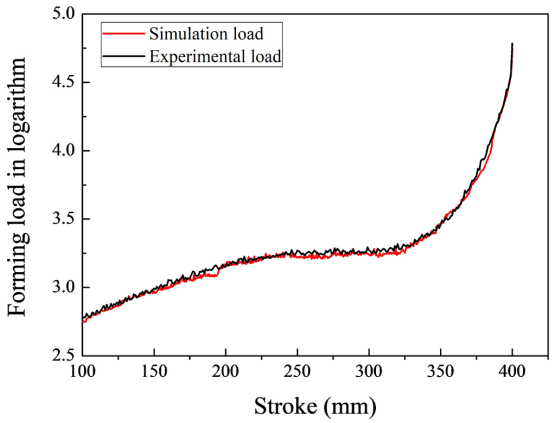

Figure 17. Logarithm load–stroke curves under experimental condition and simulation condition.

4. Conclusions

An ANN model has been developed to deal with the flow behaviors of Invar36 alloy using experimental data from hot compression tests in the temperature range of 873–1173 K and strain rate range of 0.01-10 s^{-1}. The following conclusions can be drawn:

1. The flow stress curves of Invar36 alloy show highly nonlinear characteristics. The flow stress curves at high temperature and low strain rate are characterized by a single peak following a continuous decline towards a steady state, indicating the occurrence of DRX during hot deformation. Other flow stress curves are identified by a steady state without any peak, which commonly exhibits the process of DRV.
2. The ANN model with BP algorithm for Invar36 alloy has been developed based on the experiment data from the isothermal compression tests on Gleeble 1500 thermal simulator. The developed ANN model is effective in modeling of complex hot deformation behaviors and has excellent generalization capability in a wide processing parameter range.
3. A comparative study on constitutive equation by regression method and ANN model for Invar36 alloy at strain of 0.5 was performed. Lower *AARE* value and higher *R*-value, better distribution of relative percentage error indicate a better performance of the ANN model under limited experimental conditions than that of constitutive equation by regression method.
4. The applications of ANN model on the finite element simulation have been realized and illustrated by a hot forming experiment of a V-shaped part. The great results have demonstrated that the application potentiality of the ANN model is excellent in the field of hot forming processes.

5. References

1. Chen J, Zhan XH, Xia L, Zhang D, Liu Y, Wei YH. Quantitative research on the heat affected zone of weave bead welding for Invar alloy. China Welding, 2017;26(2):18-22.
2. He S, Li CS, Zheng JJ, Ren JY, Han YH. Effect of deformation temperature on dynamic recrystallization and CSL grain boundary distribution of Fe-36%Ni invar alloy. J Mater Eng Perform. 2018;27(6):2759-65.
3. Zhao Y, Wu AP, Yao W, Wang ZM, Sato YS, Kokawa H. Microstructure and mechanical properties of Nd:YAG laser welded invar 36 alloy. Mater Sci Forum. 2011;675-677(Pt 2):739-42.
4. Serajzadeh S . Prediction of thermo-mechanical behavior during hot upsetting using neural networks. Mater Sci Eng A. 2008;472(1-2):140-7.
5. Dipti S, Sumantra M, Bhaduri AK, Venugopal S, Sivaprasad PV. Analysis and mathematical modelling of elevated temperature flow behaviour of austenitic stainless steels. Mater Sci Eng A. 2011;528(4):1937-43.
6. Zhu YC, Zeng WD, Sun Y, Feng F, Zhou YG. Artificial neural network approach to predict the flow stress in the isothermal compression of as-cast TC21 titanium alloy. Comput Mater Sci. 2011;50(5):1785-90.
7. Quan GZ, Lv WQ, Mao YP, Zhang YW, Zhou J. Prediction of flow stress in a wide temperature range involving phase transformation for as-cast Ti–6Al–2Zr–1Mo–1V alloy by artificial neural network. Mater Des. 2013;50:51-61.
8. Sheikh H, Serajzadeh S. Estimation of flow stress behavior of AA5083 using artificial neural networks with regard to dynamic strain ageing effect. J Mater Process Technol. 2008;196(1-3):115-9.
9. Malinov S, Sha W. Application of artificial neural networks for modelling correlations in titanium alloy. Mater Sci Eng A. 2004;365(1):202-11.
10. Guo Z, Malinov S, Sha W. Modelling beta transus temperature of titanium alloys using artificial neural network. Comput Mater Sci. 2005;32(1):1-12.
11. Peng WW, Zeng WD, Wang QJ, Yu HQ. Comparative study on constitutive relationship of as-cast Ti60 titanium alloy during hot deformation based on Arrhenius-type and artificial neural network models. Mater Des. 2013;51(5):95-104.
12. Quan GZ, Zou ZY, Wen HR, Pu SA, Lv WQ. A characterization of hot flow behaviors involving different softening mechanisms by ANN for As-forged Ti-10V-2Fe-3Al alloy. High-Temp Mater Process. 2015;34(7):651-65.
13. Lin YC, Zhang J, Zhong J. Application of neural networks to predict the elevated temperature flow behavior of a low alloy steel. Comput Mater Sci. 2008;43(4):752-8.
14. Quan GZ, Liang JT, Lv WQ, Wu DS, Liu YY, Luo GC, et al. A characterization for the constitutive relationships of 42CrMo high strength steel by Artificial Neural Network and its application in isothermal deformation. Mater Res. 2014;17(5):615-22.
15. Lin YC, Chen MS, Zhang J. Modeling of flow stress of 42CrMo steel under hot compression. Mater Sci Eng A. 2009;499(1-2):88-92.
16. Quan GZ, Li GS, Chen T, Wang YX, Zhang YW, Zhou J. Dynamic recrystallization kinetics of 42CrMo steel during compression at different temperatures and strain rates. Mater Sci Eng A. 2011;528(13-14):4643-51.
17. Lucon PA, Donovan RP. An artificial neural network approach to multiphase continua constitutive modeling. Compos, Part B Eng. 2007;38(7-8):817-23.
18. Chai RX, Guo C, Yu L. Two flowing stress models for hot deformation of XC45 steel at high temperature. Mater Sci Eng A. 2012;534(1):101-10.
19. Lin YC, Wen DX, Deng J, Liu G, Chen J. Constitutive models for high-temperature flow behaviors of a Ni-based superalloy. Mater Des. 2014;59(9):115-23.
20. Lin YC, Liu G, Chen MS, Zhong J. Prediction of static recrystallization in a multi-pass hot deformed low-alloy steel using artificial neural network. J Mater Process Technol. 2009;209(9):4611-6.
21. Quan GZ, Wu DS, Luo GC, Xia YF, Zhou J, Liu Q, et al. Dynamic recrystallization kinetics in α phase of as-cast Ti-6Al-2Zr-1Mo-1V alloy during compression at different temperatures and strain rates. Mater Sci Eng A. 2014;589:23-33.
22. Huang YC, Lin YC, Deng J, Liu G, Chen MS. Hot tensile deformation behaviors and constitutive model of 42CrMo steel. Mater Des. 2014;53(1):349-56.

23. Yang Z, Guo YC, Li JP, He F, Xia F, Liang MX. Plastic deformation and dynamic recrystallization behaviors of Mg-5Gd-4Y-0.5 Zn-0.5 Zr alloy. Mater Sci Eng A. 2008;485(1-2):487-91.

24. Lin YC, Chen XM. A critical review of experimental results and constitutive descriptions for metals and alloys in hot working. Mater Des. 2011;32(4):1733-59.